NANO LETTERS

pubs.acs.org/NanoLett Letter

A Paste-like Polymeric Resist with High Thermal Endurance for Vapor-Phase Bottom-Up Fabrication

Chun Li, Jiaxun Yao, Rui Xia, Haochuan Wang, Yan Shao, Ming Chen, Zixin Zhang, Lizhi Yan, Paddy Kwok Leung Chan, Xing Cheng, and Yanhao Yu*

Cite This: *Nano Lett.* 2025, 25, 3541−3548 Read Online

ACCESS | Metrics & More | Article Recommendations | Supporting Information

ABSTRACT: Bottom-up microfabrication based on vapor-phase depositions (e.g., sputtering and atomic layer deposition) requires patterning resists that can endure the parasitic thermal treatment during deposition. Conventional polymeric resists encounter removability issues due to thermally induced carbonization at the interface, while emerging molecular resists face challenges of hermeticity and shape retention in bulk. Here, we introduce a paste-like patterning resist with high interfacial and bulk thermal stability, which leads to multifaceted processing characteristics: this resist is hermetic and shape-preservable during the deposition and easily removable after the deposition. Based on a wetting-driven self-assembly process, we develop a nonphotolithographic patterning procedure for this paste resist and demonstrate high-accuracy and defect-free bottom-up patterning of dielectrics, semiconductors, and conductors. Beyond vapor-phase depositions, this resist is compatible with most manufacturing techniques, providing fruitful implications for bottom-up microfabrication.

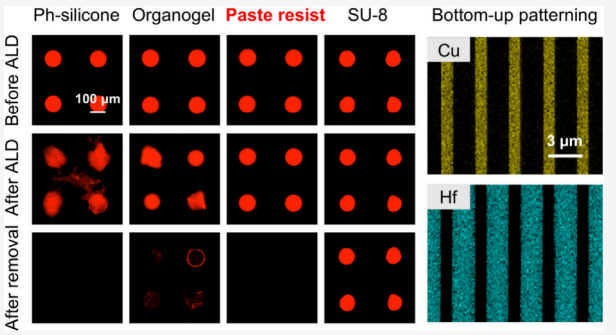

KEYWORDS: *polymeric paste, patterning resist, wetting-driven self-assembly, thermal endurance, bottom-up fabrication, atomic layer deposition*

Bottom-up microfabrication can create material patterns without lithography and etching steps, holding promise in large-area, three-dimensional, and cost-effective fabrications.[1−3] Contemporary attempts center on solution-based direct assembly of inorganic functional materials using weak forces such as van der Waals interactions or chemical affinities.[4,5] Alternatively, one can self-assemble an organic resist pattern, which is more favorable for controlling defects and scaling up over the self-assembly of inorganic patterns,[6,7] and then transform the organic to inorganic patterns by vapor-phase depositions (e.g., sputtering, chemical vapor deposition, and atomic layer deposition (ALD)). In this scenario, the organic resist has to be compatible with the thermal and physicochemical treatments induced by the vapor-phase depositions.

Relevant organic resists include resin-based photoresists,[8] metal−organic frameworks (MOFs),[9] gels,[10] and self-assembled monolayers (SAMs).[11] Resin photoresists engineered with specific reaction chemistries, represented by SU-8 and poly(methyl methacrylate) (PMMA), offer unparalleled control over pattern definition and resolution. However, these solid photoresists tightly stick to the substrate when undergoing high-temperature baking or ion bombardment in bottom-up fabrications due to interfacial bonding, requiring aggressive solvents or prolonged exposure to harsh chemicals for removal, which can potentially damage the underlying substrate or leave residues.[12−14] MOFs, gels, and SAMs were recently developed as innovative resists for specially designed processing, like EUV lithography,[15] hydrogel patterning,[16] and area-selective ALD.[17] These materials are susceptible to bulk alterations when exposed to heat, potentially leading to framework collapse,[18] phase transition,[19] or desorption.[20] The absence of a polymeric patterning resist that can maintain its processability under elevated temperatures hinders the bottom-up fabrication of micropatterns.

Paste materials, consisting of a solid matrix and liquid, have been widely used in applications including inkjet printing,[21] conductive coating,[22] adhesive,[23] ceramic craft,[24] and bone tissue engineering.[25] The compactness of the solid component provides structural integrity in the bulk, ensuring the paste maintains its form under microscopic thermal stimulus. Meanwhile, the dynamic nature of the liquid component prevents carbonization at the interface and facilitates

Received: December 4, 2024
Revised: February 18, 2025
Accepted: February 19, 2025
Published: February 21, 2025

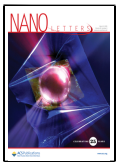

https://doi.org/10.1021/acs.nanolett.4c06189
Nano Lett. 2025, 25, 3541−3548

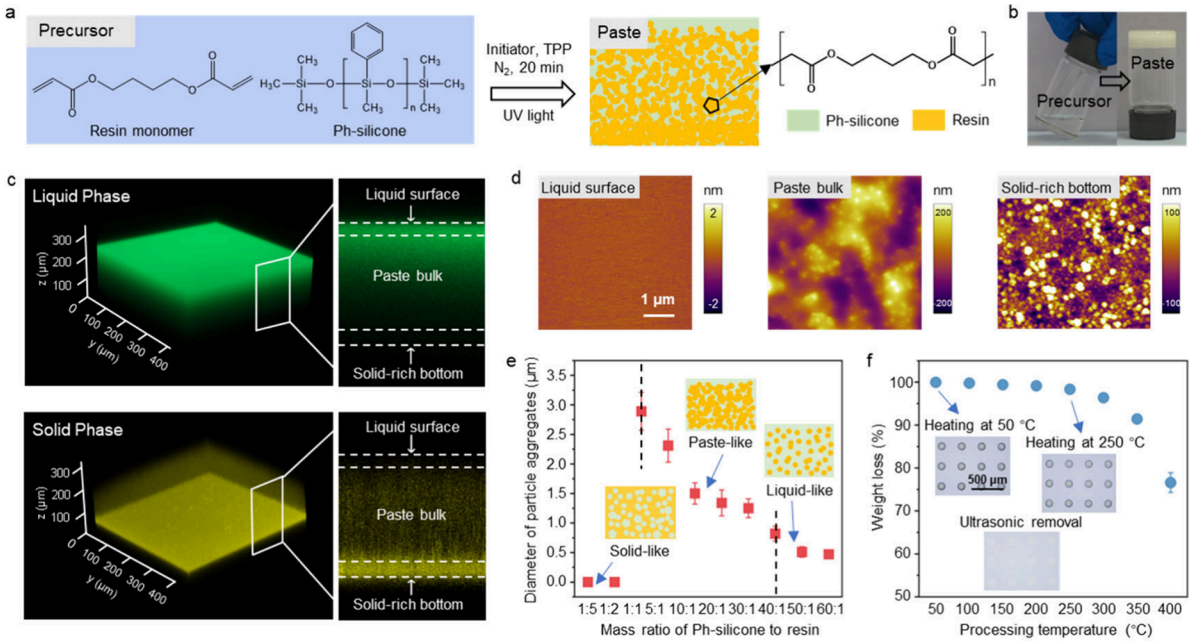

Figure 1. Design and structural characterization of the paste. (a) Synthesis of the paste by photopolymerizing double-ended resin monomers in phenyl methyl silicone oil (Ph-silicone), forming a continuous nanoparticle network with oil infused. (b) Photographs of the paste precursor solution and the as-prepared paste with a Ph-silicone to resin mass ratio of 3:1. (c) 3D confocal fluorescence images and horizontal cross-sectional views of the paste using a green dye to stain the liquid phase and an orange dye to stain the solid phase. (d) AFM topography images of the liquid surface, paste bulk, and solid-rich bottom, verifying the schematic illustration of the paste structure in (a). (e) The diameter of particle aggregates in the paste bulk as a function of the mass ratio of Ph-silicone to resin. According to the phase difference, the composites can be divided into three groups: solid-like, paste-like, and liquid-like materials. (f) The weight loss of the paste as a function of the processing temperature. Insets are optical images of a paste pattern after being sequentially heated at 50 °C for 1 h, 250 °C for 1 h, and ultrasonically cleaned in toluene for 10 min.

disassembly of the paste when subjected to macroscopic forces.[26] Motivated by this rationale, we developed a paste-like patterning resist made by photopolymerizing resin monomer in phenyl methyl silicone oil (Ph-silicone), denoted as a paste resist. The resulting resist is shape-preservable during heat-involved processing, hermetic at the molecular level, and easily disassembled after use. Combined with a wetting-driven self-assembly patterning procedure, it enables high-accuracy and defect-free patterning of oxide thin films, oxide nanowires, and metal thin films by using various microfabrication techniques, including vapor-phase depositions, reactive ion etching, and wet-chemistry processing.

Ph-silicone was selected as the liquid component, considering it is thermally stable, chemically inert, nearly nonvolatile, and miscible with carbon-based resin monomers. The resin monomer was a double-ended acrylate featuring an ultrahigh degree of cross-linking after curing, not the commonly used single-ended acrylate molecule that generates a gel network. The paste material was synthesized via free radical polymerization using a 3:1 wt % mixture of Ph-silicone oil (viscosity, 150 mPa·s) and hexanediol diacrylate (HDDA) without solvent (Figure 1a).

Different from the conventional photo-cross-linking of resin in a nitrogen atmosphere that produces a continuous film, the double-ended resin cured in Ph-silicone tends to form a homogeneous milk-white paste composed of resin nanoparticles surrounded by silicon oil (Figure 1b). The shear viscosity of the paste is more than 1 order of magnitude lower than that of the organogel and solid resin with comparable chemical composition under the same shear rate, showing significantly lower internal friction and higher flow tendency for the paste (Figure S1). The paste has a liquid surface, a paste bulk, and a solid-rich bottom, as revealed by confocal and atomic force microscopy (AFM, Figure 1c,d). The size of the individual nanoparticle is a few tens of nanometers (Figure S2). Particle aggregates with interconnections can be observed in the paste bulk (Figure 1d). The paste condition (e.g., solid-like or liquid-like) is tunable by controlling the ratio between the oil and resin, which determines the size, aggregation, and interconnection of nanoparticles (Figure 1e). The aggregate diameter in the paste bulk was inversely proportional to the mass ratio of Ph-silicone to monomer for conditions where the content of Ph-silicone exceeded that of resin monomer. However, when the monomer content was higher than that of Ph-silicone, the particle networks disappeared and were replaced by a continuous resin film with Ph-silicone droplets embedded (Figure S3a). On the other end, an excessive amount of silicone oil led to the destruction of the particle network, causing the paste to lose its structural stability and exhibit fluidity at room temperature (Figure S3b). The apposite paste with a continuous particle network can keep its weight and shape at 250 °C and was subsequently removable by ultrasonic cleaning in an organic solvent for 10 min, showing high bulk and interfacial thermal stability (Figure 1f).

To evaluate the paste as a patterning resist, we compared a series of processing properties under elevated temperatures (e.g., shape retention, removability, hermeticity, and compatibility) among four groups of materials, including a commercial SU-8 photoresist, a pristine Ph-silicone oil, the paste resist, and an organogel with a chemical composition similar to that of the paste resist. We chose prepatterned Cu on a Si wafer and plasma-enhanced ALD, both of which are commercially relevant in semiconductor manufacturing, as the exemplary

https://doi.org/10.1021/acs.nanolett.4c06189
Nano Lett. 2025, 25, 3541−3548

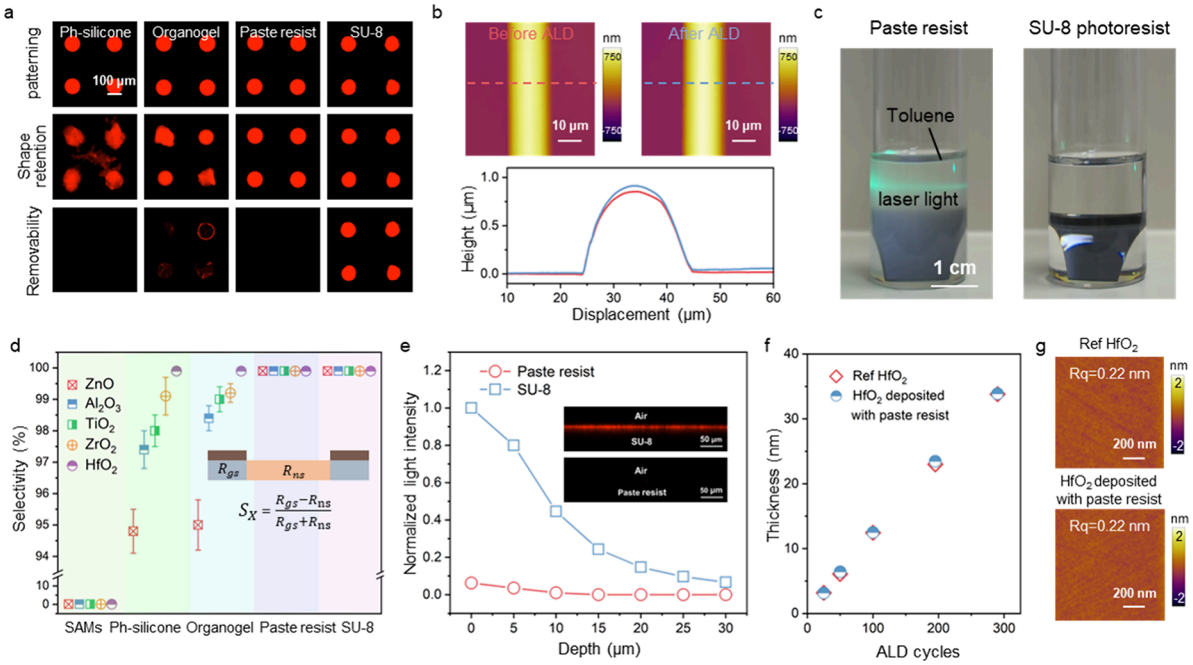

Figure 2. Processing properties of the paste resist. (a) Shape retention and removability tests: confocal fluorescence images of stained (dye: Coumarin-6, 10 nM) Ph-silicone, organogel, paste resist, and SU-8 coated on Cu surfaces (first row); their shape changes after 300 cycles of ALD HfO_2 (second row); and their residues after ALD and 10 min of ultrasonic cleaning in toluene solution (third row). (b) High-resolution characterization of shape retention: AFM topography images of paste resist before and after 300 cycles of ALD HfO_2, identifying an exactly matched line width. (c) Removability tests: paste resist (left) and SU-8 (right) on Si wafers with 300 cycles of ALD HfO_2 after ultrasonic cleaning in toluene for 5 min. GPR underwent disintegration and resin particles dispersed in toluene, resulting in a reduction of the solvent's transparency, as visualized by the light scattering. (d) Hermeticity test: selectivity of 300 ALD cycles on a prepatterned Cu−Si substrate using five different materials as the resist. They were compared under the same film thickness of 500 ± 100 nm, except for SAMs (~3 nm). Inset is the equation to calculate selectivity (S_X), where R_{gs} and R_{ns} represent the atomic composition on the growth surface (Si) and nongrowth surface (Cu), respectively. (e) Surface adsorption test: fluorescence intensity profiles (normalized concentration) as a function of depth, indicating the absorption and diffusion of water/dye molecules on the paste resist and SU-8 photoresist. Insets are cross-sectional fluorescent images after the removal of the aqueous dye solution. (f, g) Compatibility test: thickness variations (f) and AFM topography images (g) for ALD HfO_2 deposited with and without the paste resist.

substrate and microfabrication environment. Plasma-enhanced ALD covers a wide range of fabrication conditions, including temperature (100−250 °C), vacuum (0.1−10 mbar), time (1−10 h), and chemical environment (reactive metal organic molecules and oxygen plasma). The paste was found to be the only material that fulfills all of the preferred processing attributes.

The shape retention capability and postprocessing removability of a resist are two basic properties that need to be concurrently fulfilled but are usually inextricably linked, especially when thermal treatments are involved. Figure 2a shows that the mobile Ph-silicone liquid was easily removable by solvent while losing its shape after ALD. The organogel failed to maintain its geometry and left residues after cleaning. The SU-8 preserved its geometry yet stuck to the substrate after ALD, as a result of thermally induced interfacial bonding, excessive thermal cross-linking, and the coverage of oxide film on the SU-8 surface that prevents removing agents from functioning (Figure S4). In contrast, the paste resist clearly maintained its shape after ALD and was easily removed by ultrasonication in solvent. At the micrometer scale, no edge movement was detectable under AFM for a paste resist that was continuously heated at 150 °C for nearly 10 h in ALD equipment (Figure 2b). The natural curvature observed in the paste resist stripes arises from the minimization of surface tension of the liquid precursor. This curvature can be harnessed for creating functional micro- and nanostructures that enhance light capture (e.g., microlens arrays)[27] and control liquid flow (e.g., microfluidic channels).[28] The simultaneous possession of stability and removability originates from the unique paste structure, where the solid matrix constructed by the resin nanoparticles effectively constrained the mobility of the silicone oil, making the oil immune to microscopic stimuli (Figure S5). In the other direction, the oil environment prevents the formation of covalent bonds between the resin nanoparticles and the substrate during heating. It also weakens the interconnection between resin nanoparticles and aggregates, enabling a rapid structural disassembly when subjected to macroscopic forces like ultrasonication (Figure 2c). Furthermore, the oil residue underneath the paste resist helps any insoluble resin nanoparticle leftovers slip off the substrate.

Hermeticity refers to the barrier performance of a resist that determines the isolation degree of the underneath surface from the fabrication environment, which is an essential point to ensure that the resist-covered area is defect-free. The field of area-selective ALD introduced the deposition selectivity to evaluate this aspect,[29] namely the selectivity $S_X = (R_{gs} - R_{ns})/(R_{gs} + R_{ns})$, where R_{gs} and R_{ns} represent the atomic composition on the growth surface and nongrowth surface, respectively. The semiconductor industry requires selectivity to be above 99.999% to avoid potential influence from defects.[30] As shown in Figure 2d and Figure S6, the selectivity of five ALD oxides (i.e., HfO_2, ZrO_2, TiO_2, Al_2O_3, and ZnO) on the

https://doi.org/10.1021/acs.nanolett.4c06189
Nano Lett. 2025, 25, 3541−3548

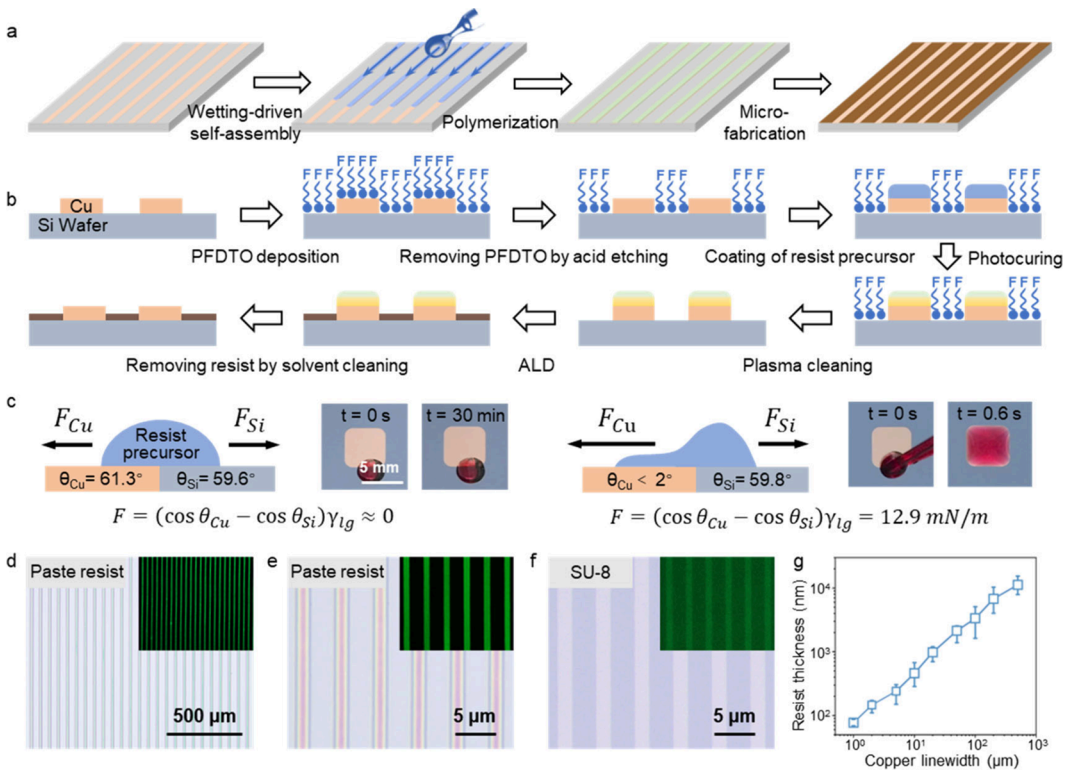

Figure 3. Wetting-driven self-assembly patterning of the paste resist. (a) Three sequential processes for self-assembly patterning: wetting-driven selective coating, polymerization under UV light, and microfabrication. (b) Processing steps for the wetting-driven patterning of the paste resist on a Cu−Si substrate, including surface treatments of the substrate, self-alignment of the paste resist, and removal of the paste resist after ALD. (c) Schematic of the self-assembly mechanism of the paste resist at the Cu−Si boundary. The wetting difference of the resist precursor solution on Cu and Si surfaces (represented by the contact angles θ_{Cu} and θ_{Si}) provides the driving force (F) for self-assembly. γ_{lg} is the surface tension between the precursor and air. (d−f) Optical and corresponding confocal fluorescence images (insets, dyed by Coumarin-6, 10 nM) of the self-assembled paste patterns (d, e) and a uniformly coated SU-8 film (f) on Cu−Si substrates. The samples were prepared by a single-step blade coating of the paste resist precursor or SU-8 solution, followed by a UV-curing process. The widths of Cu strips are 20 μm in (d) and 2 μm in (e, f). (g) Thickness variation of self-assembled paste resist films on Cu strips as a function of the Cu line width. The data were collected from four independent measurements.

samples of SAMs (the resist commonly used in area-selective ALD), Ph-silicone, and organogel was far from the industry requirement after 300 cycles of ALD. The selectivity of all oxides using the paste resist reached 99.9%, the detection limit of X-ray photoelectron spectroscopy (XPS), comparable with that of SU-8. The XPS depth profile analysis accordingly shows that the primary infiltration depth of ALD precursors inside the paste resist was only about a few tens of percentages of the total film thickness (Figure S7). The high hermeticity of the paste resist was presumably a combined outcome of the discontinuous diffusion pathway implemented by the paste bulk, the weak surface adsorption induced by the oil coverage, and the largely reduced free volume in the solid-rich layer at the bottom. The local vibration and low polarity of the oily molecules make them strongly immune to chemical and/or physical adsorption of polar species in contrast to the apparent surface adsorptions on a solid surface, as revealed by a dye adsorption test (Figure 2e) and XPS depth profiling (Figure S8).

There is a natural concern of whether the quality of oxides will be affected when introducing liquid contents into ALD. We therefore compared the growth rate (Figure 2f), surface roughness (Figure 2g), chemical composition, and dielectric property (Figure S9) of ALD HfO_2 thin films obtained with and without the presence of the paste resist. Due to the excellent thermal stability of Ph-silicone oil (Figure S10), the ALD films deposited with and without the paste resist have the same growth rates of ∼1.1 Å/cycle and surface roughness of 0.22 nm, consistent with reported ALD HfO_2 films.[31] Moreover, according to the yield capacitance measurement and XPS analysis, no significant difference was found in terms of the dielectric constant and chemical state among these HfO_2 films, evidencing the high compatibility of the paste resist with the complex ALD environment. Similar trends were observed on other oxides. For example, the film properties of ALD TiO_2 remained high regardless of the presence of the paste resist (surface roughness of <0.5 nm and water vapor transmission rate of <0.1 $g{\cdot}m^{-1}{\cdot}day^{-1}$) (Figure S11).

The paste resist can form high-accuracy patterns through a wetting-driven self-assembly process on the surface of Cu strips prepatterned on a Si wafer (Figure 3a). This approach utilized the surface energy difference between Cu and Si to align the paste precursor with the Cu area. To maximize the surface energy difference, a lipophobic fluorinated SAMs layer was selectively introduced on the Si surface via sequentially immersing the substrate in a 1*H*,1*H*,2*H*,2*H*-perfluorodecyltrimethoxysilane (PFDTO) toluene solution for 12 h and in a glacial acetic acid solution for 3 min (Figure 3b). The PFDTO treatment increased the oil contact angle (OCA) of Cu and Si surfaces to ∼60°. The acid soaking removed the PFDTO layer from the Cu surface by etching out the native CuO while leaving the Si surface intact. Consequently, the Cu surface

https://doi.org/10.1021/acs.nanolett.4c06189
Nano Lett. 2025, 25, 3541−3548

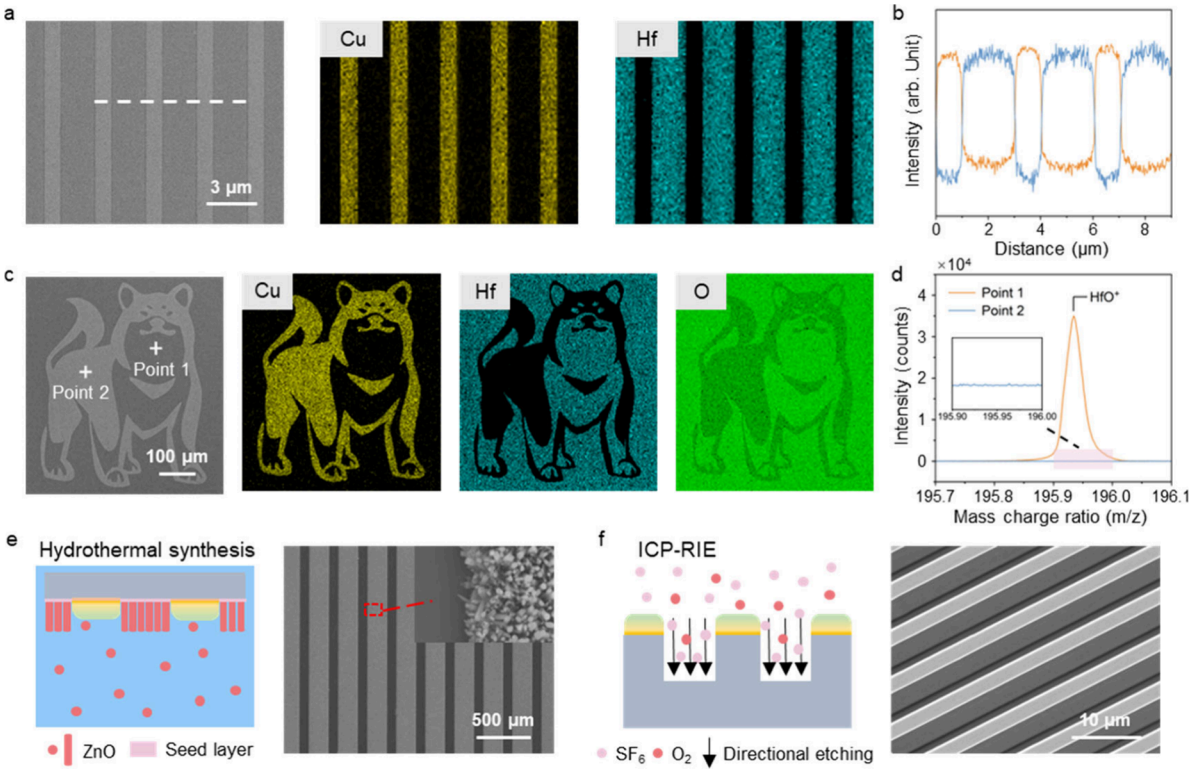

Figure 4. Bottom-up fabrication of oxide patterns using the paste resist. (a) High-resolution patterning: top-view SEM image and corresponding Auger elemental mappings for a 300 cycle ALD HfO_2 pattern created on a Cu−Si substrate using the wetting-based self-assembly approach shown in Figure 3b. (b) A line scan of Hf and Cu signals for the region highlighted by the white dotted line in (a), showing an exact line width of 1 and 2 μm for Cu and Hf, respectively. (c) Top-view SEM image and corresponding AES elemental mappings for a 300 cycle ALD HfO_2 pattern with a "dog" pattern. (d) ToF-SIMS area analysis of HfO^+ secondary ions conducted with a size of 10 × 10 μm on the HfO_2-coated Si surface located at point 1 and the Cu surface located at point 2 in the SEM image in (c). Inset is the enlarged view of point 2, showing no Hf signal detected. (e) Schematic (left) and corresponding SEM image of obtained samples (right) for using the paste resist in the hydrothermal growth of ZnO nanowires. The inset shows the ZnO nanowires selectively grown on the Si surface. (f) Schematic (left) and corresponding SEM image (right) for using the paste resist in reactive ion etching. The etching depth was ∼8 μm.

became lipophilic (OCA < 2°), and the Si surface remained lipophobic (OCA ∼ 60°) (Figure S12). With this contrast on the wetting property, the precursor solution, which was composed of resin monomer and Ph-silicone oil, can neatly spread following the Cu pattern via a dip coating, a single-step blade coating, or a spin coating process. The resist pattern was obtained after photocuring the precursor and removing the PFDTO molecules by plasma cleaning (Figure S13).

The driving force for the selective spreading can be described by[32] $F = (\cos\theta_{Cu} - \cos\theta_{Si})\gamma_{lg}$, where θ_{Cu} and θ_{Si} are the contact angles of the paste precursor on Cu and Si surfaces, respectively ($\theta_{Cu} = 2°$, $\theta_{Si} = 59.8°$ in our system), and γ_{lg} is the surface tension at the liquid−gas interface ($\gamma_{lg} = 26$ mN·m^{-1} in our system). With a measured F of 12.9 mN·m^{-1} (Figure 3c), the precursor droplet (dyed with Oil Red O) located at the Cu−Si edge fully spread across the entire 5 × 5 mm Cu square within 0.6 s, outlining the high efficiency of this self-assembly process. Conversely, there was no observable movement or spreading when $F = 0$ mN·m^{-1}.

The self-assembly performance of the paste resist was further evaluated on microscale patterns with help from a green fluorescent dye mixed with the precursor. As shown in Figure 3d, the precursor was well spread along the Cu strips that have a line width of 20 μm and a pitch size of 40 μm on the PFDTO-treated Si substrate. In principle, this self-aligning patterning method has no size limitation. As a proof of concept, we demonstrated uniform patterning of the paste resist on a 4 in. Si wafer with prepatterned 20 μm wide Cu strips (Figure S14). When the Cu line width and pitch size shrank to 2 and 3 μm, respectively, the paste resist was still able to self-pattern on the Cu surface with a uniform coverage and a clean edge, as indicated by the green lines in the confocal optical image (Figure 3e). The SU-8 photoresist disregarded the chemical treatments on the Cu−Si substrate and covered the entire surface with no pattern formed, likely due to the low molecular mobility, considering its long molecular chains (Figure 3f). The 2 μm scale resolution is comparable to that of conventional contact photolithography.[33] The paste resist can also be patterned on a bare silicon substrate with controlled surface wettability via the microcontact printing method (Figure S15), verifying its versatility in creating patterns on different substrates.

Further pushing the resolution to the nanometer scale was limited by the dependence of the film thickness of the paste resist on the line width of the Cu strips. The AFM and step profiler measurements disclose a linear relationship between the film thickness of the paste resist and Cu width with a slope of 1:20 (Figure 3g). That means that the resist film would be as thin as 5 nm when the Cu strip was 100 nm in width. The ultrathin film brought strong interfacial effects that substantially hinder the mobility of liquid precursors and erase its self-assembly feature, making nanometer patterning inaccessible at the moment. Reducing the viscosity can improve the spreading and self-assembly abilities of the precursor solution, potentially

https://doi.org/10.1021/acs.nanolett.4c06189
Nano Lett. 2025, 25, 3541−3548

leading to higher resolution. For a line width of 3 μm and below, decreasing the viscosity of the precursor solution brought a marginal resolution improvement and considerable patterning nonuniformity, consistent with the resolution limit observed in reported wetting-based patterning technologies.[34,35] Nanometer resolution may be accessible by introducing photolithography or other nonwetting-based patterning techniques. However, the chemical and optical properties of the paste resist need to be carefully tuned or even redesigned to balance the spatial resolution and thermal stability.

The multifaceted processing properties of the paste allow the self-assembled resist patterns to be transformed to oxide patterns through direct vapor-phase deposition. For example, we conducted 300 cycles of ALD HfO_2 at 150 °C on a Cu−Si substrate (1 μm Cu strips with a 2 μm pitch size) that has the self-assembled paste resist protecting the Cu area. After the deposition, the resist was removed by solvent ultrasonication, creating an oxide pattern covering only the Si surface. The Auger electron spectroscopy (AES) elemental mapping and line scan identified high-contrast Cu and Hf signals arranged in alternating strips with a line width of 1 and 2 μm, respectively, evidencing that HfO_2 was merely coated on the Si surface and did not overlap with Cu (Figure 4a,b). For the case of a 20 μm Cu width and 40 μm pitch size, the edge roughness of the ALD HfO_2 was <50 nm, corresponding to a deposition accuracy of 99.75%. There was an uncoated gap line with a width of ∼100 nm between the Cu and HfO_2 areas (Figure S16), which could be a favorable design for advanced transistors.[36] The gap was presumably caused by overcoating of the liquid precursor along the corner space created by the height of the Cu strips (50 nm above the Si surface). The gap would be avoidable by using coplanar Cu patterns on Si substrates.[37]

In addition to periodic strips, the paste resist applies to Cu−Si substrates with sophisticated patterns, for example, a "dog" contour that incorporates curves, angles, and variations in size. Through a procedure similar to that shown in Figure 3b, the ALD HfO_2 with a thickness of 33 nm was selectively coated on the Si surface with high accuracy following the designed pattern, as shown by the mutually exclusive Cu and Hf signals on the AES mapping (Figure 4c). The oxygen signal with a relatively low intensity was observed on the Cu surface due to the native CuO.

We further introduced time-of-flight secondary ion mass spectrometry (ToF-SIMS) to disclose any trace amount of HfO_2 that may penetrate through the paste resist and deposit on the Cu surface. The detection limit of ToF-SIMS is below 1 ppm, at least 3 orders of magnitude lower than that of XPS and AES. As shown in Figure 4d, no HfO^+ signal was detected on the Cu surface by ToF-SIMS. That indicates the defect level on the resist-created patterns could be lower than 0.00001%, approaching the requirement of the semiconductor industry.

Beyond ALD, the newly developed paste resist applies to a variety of manufacturing techniques, such as wet-chemistry processing (Figure 4e), reactive ion etching (Figure 4f), electron beam evaporation, and magnetron sputtering (Figure S17). During the entire process of hydrothermal growth of ZnO nanowires, the paste resist exhibited high stability and did not undergo detachment or dispersion in the aqueous solution. Comparable reliability and patterning performance of the paste resist were obtained in inductively coupled plasma reactive ion etching (ICP-RIE) for fabricating Si trenches, e-beam deposition for coating an Al film, and magnetron sputtering for coating a Pt film.

In summary, we have developed a new paste resist that is shape-preservable during thermal processing, easily removable after use, hermetic at the molecular level, capable of self-assembling to prepatterns with high accuracy and resolution, and broadly applicable to different microfabrication techniques. The otherwise impossible integration of functions was a consequence of the unique structure featuring a continuous nanoparticle network infused with a Ph-silicone oil. This paste resist can self-assemble on the targeted areas with a high accuracy of 99.75% at a scale of 1 μm based on a wetting-driven method. The impurity content at the resist-protected surface was below 1 ppm (the detection limit of ToF-SIMS) after 300 cycles of ALD HfO_2 coating. Furthermore, the paste resist is compatible with a wide range of manufacturing methods. Nanoscale patterning is inaccessible at the moment due to the intrinsic limitation of the wetting-driven self-assembly process. Other patterning approaches (e.g., photolithography and surface-induced lithography) can potentially break this resolution limit for the paste resist and are currently under development.

■ ASSOCIATED CONTENT

Supporting Information

The Supporting Information is available free of charge at https://pubs.acs.org/doi/10.1021/acs.nanolett.4c06189.

Materials, synthesis methods, experimental and characterization details, additional characterization data (SEM, EDS, AFM, XPS, TGA, AES), optical images, rheological measurement, nanoindentation analysis, XPS depth profiling, and dielectric and WVTR measurements of ALD films (PDF)

■ AUTHOR INFORMATION

Corresponding Author

Yanhao Yu − *Department of Materials Science and Engineering and Institute of Innovative Materials, Guangdong Provincial Key Laboratory of Sustainable Biomimetic Materials and Green Energy, Southern University of Science and Technology, Shenzhen 518055, China;* orcid.org/0000-0003-2494-3006; Email: yuyh@sustech.edu.cn

Authors

Chun Li − *Department of Materials Science and Engineering, Southern University of Science and Technology, Shenzhen 518055, China; Harbin Institute of Technology, Harbin 150080, China*

Jiaxun Yao − *Department of Materials Science and Engineering, Southern University of Science and Technology, Shenzhen 518055, China*

Rui Xia − *Department of Materials Science and Engineering, Southern University of Science and Technology, Shenzhen 518055, China*

Haochuan Wang − *Department of Materials Science and Engineering, Southern University of Science and Technology, Shenzhen 518055, China;* orcid.org/0009-0009-0130-0826

Yan Shao − *Department of Materials Science and Engineering, Southern University of Science and Technology, Shenzhen 518055, China*

https://doi.org/10.1021/acs.nanolett.4c06189
Nano Lett. 2025, 25, 3541−3548

Ming Chen − *Department of Materials Science and Engineering and Shenzhen Key Laboratory for Nanoimprint Technology, Southern University of Science and Technology, Shenzhen 518055, China*

Zixin Zhang − *Department of Materials Science and Engineering, Southern University of Science and Technology, Shenzhen 518055, China*

Lizhi Yan − *Department of Mechanical Engineering, The University of Hong Kong, Hong Kong 999077, China*

Paddy Kwok Leung Chan − *Department of Mechanical Engineering, The University of Hong Kong, Hong Kong 999077, China; Advanced Biomedical Instrumentation Centre, Shatin, Hong Kong 999077, China;* orcid.org/0000-0002-3166-2192

Xing Cheng − *Department of Materials Science and Engineering and Shenzhen Key Laboratory for Nanoimprint Technology, Southern University of Science and Technology, Shenzhen 518055, China*

Complete contact information is available at: https://pubs.acs.org/10.1021/acs.nanolett.4c06189

Notes

The authors declare no competing financial interest.

■ ACKNOWLEDGMENTS

This work was supported by the National Natural Science Foundation of China (No. 52272299), Natural Science Foundation of Guangdong Province, China (No. 2024A1515012366), Guangdong Provincial Key Laboratory of Sustainable Biomimetic Materials and Green Energy (2024B1212010003), High Level of Special Funds (G03050K002), and the Shenzhen Science and Technology Innovation Commission (No. 20220815141329003 and KQTD20180411143514543). Y.S. was supported by the National Natural Science Foundation of China (No. 52303107). We thank the Vacuum Interconnected Nanotech Workstation in Suzhou, China, for providing assistance on AES and ToF-SIMS characterizations.

■ REFERENCES

(1) Kwon, Y. A.; Kim, J.; Jo, S. B.; Roe, D. G.; Rhee, D.; Song, Y.; Kang, B.; Kim, D.; Kim, J.; Kim, D. W.; Kang, M. S.; Kang, J.; Cho, J. H. Wafer-scale transistor arrays fabricated using slot-die printing of molybdenum disulfide and sodium-embedded alumina. *Nat. Electron.* **2023**, *6*, 443.

(2) Li, T.; Miao, J.; Fu, X.; Song, B.; Cai, B.; Ge, X.; Zhou, X.; Zhou, P.; Wang, X.; Jariwala, D.; Hu, W. Reconfigurable, non-volatile neuromorphic photovoltaics. *Nat. Nanotechnol.* **2023**, *18*, 1303.

(3) Wang, W.; Jiang, Y.; Zhong, D.; Zhang, Z.; Choudhury, S.; Lai, J.-C.; Gong, H.; Niu, S.; Yan, X.; Zheng, Y.; Shih, C.-C.; Ning, R.; Lin, Q.; Li, D.; Kim, Y.-H.; Kim, J.; Wang, Y.-X.; Zhao, C.; Xu, C.; Ji, X.; Nishio, Y.; Lyu, H.; Tok, J. B.-H.; BAO, Z. Neuromorphic sensorimotor loop embodied by monolithically integrated, low-voltage, soft e-skin. *Science* **2023**, *380*, 735.

(4) Yeh, C.-C.; Zan, H.-W.; Soppera, O. Solution-Based Micro-and Nanoscale Metal Oxide Structures Formed by Direct Patterning for Electro-Optical Applications. *Adv. Mater.* **2018**, *30*, No. 1800923.

(5) Baek, S.; Jeong, S.; Ban, H. W.; Ryu, J.; Kim, Y.; Gu, D. H.; Son, C.; Yoon, T.-S.; Lee, J.; Son, J. S. Nanoscale Vertical Resolution in Optical Printing of Inorganic Nanoparticles. *ACS Nano* **2023**, *17*, 24268.

(6) Chen, R.; Wang, X.; Li, X.; Wang, H.; He, M.; Yang, L.; Guo, Q.; Zhang, S.; Zhao, Y.; Li, Y.; Liu, Y.; Wei, D. A comprehensive nano-interpenetrating semiconducting photoresist toward all-photolithography organic electronics. *Sci. Adv.* **2021**, *7*, No. eabg0659.

(7) Zheng, Y.-Q.; Liu, Y.; Zhong, D.; Nikzad, S.; Liu, S.; Yu, Z.; Liu, D.; Wu, H.-C.; Zhu, C.; Li, J.; Tran, H.; Tok, J. B.-H.; Bao, Z. Monolithic optical microlithography of high-density elastic circuits. *Science* **2021**, *373*, 88.

(8) Wang, B.; Huang, W.; Lee, S.; Huang, L.; Wang, Z.; Chen, Y.; Chen, Z.; Feng, L.-W.; Wang, G.; Yokota, T.; Someya, T.; Marks, T. J.; Facchetti, A. Foundry-compatible high-resolution patterning of vertically phase-separated semiconducting films for ultraflexible organic electronics. *Nat. Commun.* **2021**, *12*, 4937.

(9) Tian, X.; Li, F.; Tang, Z.; Wang, S.; Weng, K.; Liu, D.; Lu, S.; Liu, W.; Fu, Z.; Li, W.; Qiu, H.; Tu, M.; Zhang, H.; Li, J. Crosslinking-induced patterning of MOFs by direct photo-and electron-beam lithography. *Nat. Commun.* **2024**, *15*, 2920.

(10) Scheiger, J. M.; Li, S.; Brehm, M.; Bartschat, A.; Theato, P.; Levkin, P. A. Inherently UV photodegradable poly (methacrylate) gels. *Adv. Funct. Mater.* **2021**, *31*, No. 2105681.

(11) Li, Y.; Qi, Z.; Lan, Y.; Cao, K.; Wen, Y.; Zhang, J.; Gu, E.; Long, J.; Yan, J.; Shan, B.; Chen, R. Self-aligned patterning of tantalum oxide on Cu/SiO_2 through redox-coupled inherently selective atomic layer deposition. *Nat. Commun.* **2023**, *14*, 4493.

(12) Liu, G.; Tian, Y.; Kan, Y. Fabrication of high-aspect-ratio microstructures using SU8 photoresist. *Microsyst. Technol.* **2005**, *11*, 343.

(13) Dentinger, P. M.; Clift, W. M.; Goods, S. H. Removal of SU-8 photoresist for thick film applications. *Microelectron. Eng.* **2002**, *61*, 993.

(14) Chung, S.; Park, S. Effects of temperature on mechanical properties of SU-8 photoresist material. *J. Mech. Sci. Technol.* **2013**, *27*, 2701.

(15) Xu, H.; Sakai, K.; Kasahara, K.; Kosma, V.; Yang, K.; Herbol, H. C.; Odent, J.; Clancy, P.; Giannelis, E. P.; Ober, C. K. Metal−organic framework-inspired metal-containing clusters for high-resolution patterning. *Chem. Mater.* **2018**, *30*, 4124.

(16) Liu, Y.; Liu, J.; Chen, S.; Lei, T.; Kim, Y.; Niu, S.; Wang, H.; Wang, X.; Foudeh, A. M.; Tok, J. B.-H.; Bao, Z. Soft and elastic hydrogel-based microelectronics for localized low-voltage neuromodulation. *Nat. Biomed. Eng.* **2019**, *3*, 58.

(17) Cao, K.; Cai, J.; Chen, R. Inherently selective atomic layer deposition and applications. *Chem. Mater.* **2020**, *32*, 2195.

(18) Wu, S.-F.; Yuan, B.-Z.; Wang, L.-W. MOF−ammonia working pairs in thermal energy conversion and storage. *Nat. Rev. Mater.* **2023**, *8*, 636.

(19) Yu, A. C.; Lian, H.; Kong, X.; Lopez Hernandez, H.; Qin, J.; Appel, E. A. Physical networks from entropy-driven non-covalent interactions. *Nat. Commun.* **2021**, *12*, 746.

(20) Mackus, A. J. M.; Merkx, M. J. M.; Kessels, W. M. M. From the bottom-up: toward area-selective atomic layer deposition with high selectivity. *Chem. Mater.* **2019**, *31*, 2.

(21) Can, T. T. T.; Nguyen, T. C.; Choi, W.-S. High-viscosity copper paste patterning and application to thin-film transistors using electrohydrodynamic jet printing. *Adv. Eng. Mater.* **2020**, *22*, No. 1901384.

(22) Wang, F.; Liu, H.; Ou, J.; Li, W. Fast fabrication of superhydrophobic surfaces on hardened cement paste using sodium laurate aqueous solution. *Constr. Build. Mater.* **2021**, *278*, No. 122385.

(23) Yuk, H.; Wu, J.; Sarrafian, T. L.; Mao, X.; Varela, C. E.; Roche, E. T.; Griffiths, L. G.; Nabzdyk, C. S.; Zhao, X. Rapid and coagulation-independent haemostatic sealing by a paste inspired by barnacle glue. *Nat. Biomed. Eng.* **2021**, *5*, 1131.

(24) Heule, M.; Vuillemin, S.; Gauckler, L. J. Powder-based ceramic meso-and microscale fabrication processes. *Adv. Mater.* **2003**, *15*, 1237.

(25) Liu, Z.; Shao, C.; Jin, B.; Zhang, Z.; Zhao, Y.; Xu, X.; Tang, R. Crosslinking ionic oligomers as conformable precursors to calcium carbonate. *Nature* **2019**, *574*, 394.

(26) Scheiger, J. M.; Kuzina, M. A.; Eigenbrod, M.; Wu, Y.; Wang, F.; Heißler, S.; Hardt, S.; Nestler, B.; Levkin, P. A. Liquid wells as self-

healing, functional analogues to solid vessels. *Adv. Mater.* **2021**, *33*, No. 2100117.
(27) Wu, M.-H.; Whitesides, G. M. Fabrication of two-dimensional arrays of microlenses and their applications in photolithography. *J. Micromech. Microeng.* **2002**, *12*, 747.
(28) Battat, S.; Weitz, D. A.; Whitesides, G. M. Nonlinear phenomena in microfluidics. *Chem. Rev.* **2022**, *122*, 6921.
(29) Bobb-Semple, D.; Nardi, K. L.; Draeger, N.; Hausmann, D. M.; Bent, S. F. Area-selective atomic layer deposition assisted by self-assembled monolayers: a comparison of Cu, Co, W, and Ru. *Chem. Mater.* **2019**, *31*, 1635−1645.
(30) Karasulu, B.; Roozeboom, F.; Mameli, A. High-throughput area-selective spatial atomic layer deposition of SiO_2 with interleaved small molecule inhibitors and integrated back-etch correction for low defectivity. *Adv. Mater.* **2023**, *35*, No. 2301204.
(31) Jarvis, K. L.; Evans, P. J.; Nelson, A.; Triani, G. Comparisons of alumina barrier films deposited by thermal and plasma atomic layer deposition. *Mater. Today Chem.* **2019**, *11*, 8.
(32) Quéré, D. Wetting and roughness. *Annu. Rev. Mater. Res.* **2008**, *38*, 71.
(33) Fruncillo, S.; Su, X.; Liu, H.; Wong, L. S. Lithographic processes for the scalable fabrication of micro-and nanostructures for biochips and biosensors. *ACS Sensors* **2021**, *6*, 2002.
(34) Wan, X.; Xu, X.; Liu, X.; Jia, L.; He, X.; Wang, S. A Wetting-Enabled-Transfer (WET) strategy for precise surface patterning of organohydrogels. *Adv. Mater.* **2021**, *33*, No. 2008557.
(35) Tian, D.; Song, Y.; Jiang, L. Patterning of controllable surface wettability for printing techniques. *Chem. Soc. Rev.* **2013**, *42*, 5184.
(36) Avrutsky, I.; Soref, R.; Buchwald, W. Sub-wavelength plasmonic modes in a conductor-gap-dielectric system with a nanoscale gap. *Opt. Express* **2010**, *18*, 348.
(37) Pattison, T. G.; Hess, A. E.; Arellano, N.; Lanzillo, N.; Nguyen, S.; Bui, H.; Rettner, C.; Truong, H.; Friz, A.; Topuria, T.; Fong, A.; Hughes, B.; Tek, A. T.; DeSilva, A.; Miller, R. D.; Qiao, G. G.; Wojtecki, R. J. Surface initiated polymer thin films for the area selective deposition and etching of metal oxides. *ACS Nano* **2020**, *14*, 4276.

https://doi.org/10.1021/acs.nanolett.4c06189
Nano Lett. 2025, 25, 3541−3548